# Patterned vegetation, tipping points, and the rate of climate change

Yuxin Chen*, Theodore Kolokolnikov†, Justin Tzou† and Chunyi Gai†

(Dated: May 22, 2015)

When faced with slowly depleting resources (such as decrease in precipitation due to climate change), complex ecological systems are prone to sudden irreversible changes (such as desertification) as the resource level dips below a tipping point of the system. A possible coping mechanism is the formation of spatial patterns, which allows for concentration of sparse resources and the survival of the species within "ecological niches" even below the tipping point of the homogeneous vegetation state. However, if the change in resource availability is too sudden, the system may not have time to transition to the patterned state and will pass through the tipping point instead, leading to extinction. We argue that the deciding factors are the speed of resource depletion and the amount of the background noise (seasonal climate changes) in the system. We illustrate this phenomenon on a model of patterned vegetation. Our analysis underscores the importance of, and the interplay between, the speed of climate change, heterogeneity of the environment, and the amount of seasonal variability.

Climate change – both anthropogenic and natural – poses multiple pressures on earth ecosystems. While the earth's climate has undergone many drastic changes in its history, the rate at which the current human-induced changes are occurring is unmatched in recent history going back at least 60 million years [1]. Just in the last century, CO2 levels in the atmosphere have increased by 50%, and are expected to double by 2050 [2]. This rate of increase is more than 200 times the fastest historical rates of at least the last 800,000 years, as measured by ice cores [3]. Similarly, the acidification of oceans is taking place at breakneck speed, likely unparalleled in earth's known history [4–6].

Large swings in earth's climate are not unprecedented, and life has been able to adapt to such swings more or less successfully in the past. The question is whether a species is resilient enough not just to the *changes* in environment, but to the *speed* with which these changes occur [7–11]. It is widely accepted that anthropogenic climate change is mainly responsible for increasingly fast swings in precipitation and other weather parameters [2, 12–15]. Many ecosystems can be very sensitive to sudden shifts in environmental conditions that can trigger critical transitions as a result of crossing a tipping point, leading to drastic changes in population density and even extinctions [11, 16–21].

The speed of climate change is especially important for an ecosystem that is already under stress, such as vegetation in arid and semi-arid environments, where a relatively small change in precipitation can have a very large impact [23]. One of the mechanisms by which the vegetation in such environments adapts is by growing in patches, leaving areas of barren land interspersed with localized patches or stripes of vegetation where it can conserve resources [11, 24–30]. However, it takes time for plants to adjust to reduced precipitation by forming patches. If the environmental changes occur too rapidly, vegetation may be unable to form these niches and face extinction. This pheonomenon was recently illustrated numerically in [11], where it was noted in §4.2 that "at high rates of change, desertification can take place at rainfall levels for which stable patterned states still exist". They used a modified version of vegetation pattern formation system introduced by Klausmeier [25]. It is a reaction-advection-diffusion system that couples plant density $n(x,t)$ to soil water concentration $w(x,t)$, and has the following non-dimensional form:

$$\frac{\partial n}{\partial t} = wn^2 - n + \delta\frac{\partial^2 n}{\partial x^2}, \tag{1a}$$

$$b\frac{\partial w}{\partial t} = a - w - wn^2 + c\frac{\partial w}{\partial x} + d\frac{\partial^2 w}{\partial x^2}\,. \tag{1b}$$

Critically, for the existence of spatially heterogeneous states, the model includes spatial terms corresponding to diffusion of water within soil ($d\partial^2 w/\partial x^2$), downhill water flow ($c\partial w/\partial x$), as well as the spread of plants ($\delta\partial^2 n/\partial x^2$). The parameter $a$ represents the precipitation rate. Parameter $b$ represents the differing timescales in changes in water level (in days, say) versus those in plant density (in months). For illustration purposes, we consider here the limit $c = 0$ (flat ground) in one dimension, corresponding to the well-known Gray-Scott model [31]; the more general case exhibits the same behaviour.

To understand the effect of the speed of precipitation changes, we consider the case in which precipitation is slowly decreased in time and fluctuates with small noise. That is, we let

$$a = a_0 - \varepsilon t + \text{noise}, \tag{2}$$

with $0 < \varepsilon \ll 1$. The initial precipitation $a_0$ is assumed to be sufficiently large so that the system has full vegetation cover (corresponding to the nontrivial spatially homogeneous state) when $a = a_0$. Here, $\varepsilon$ is a small parameter

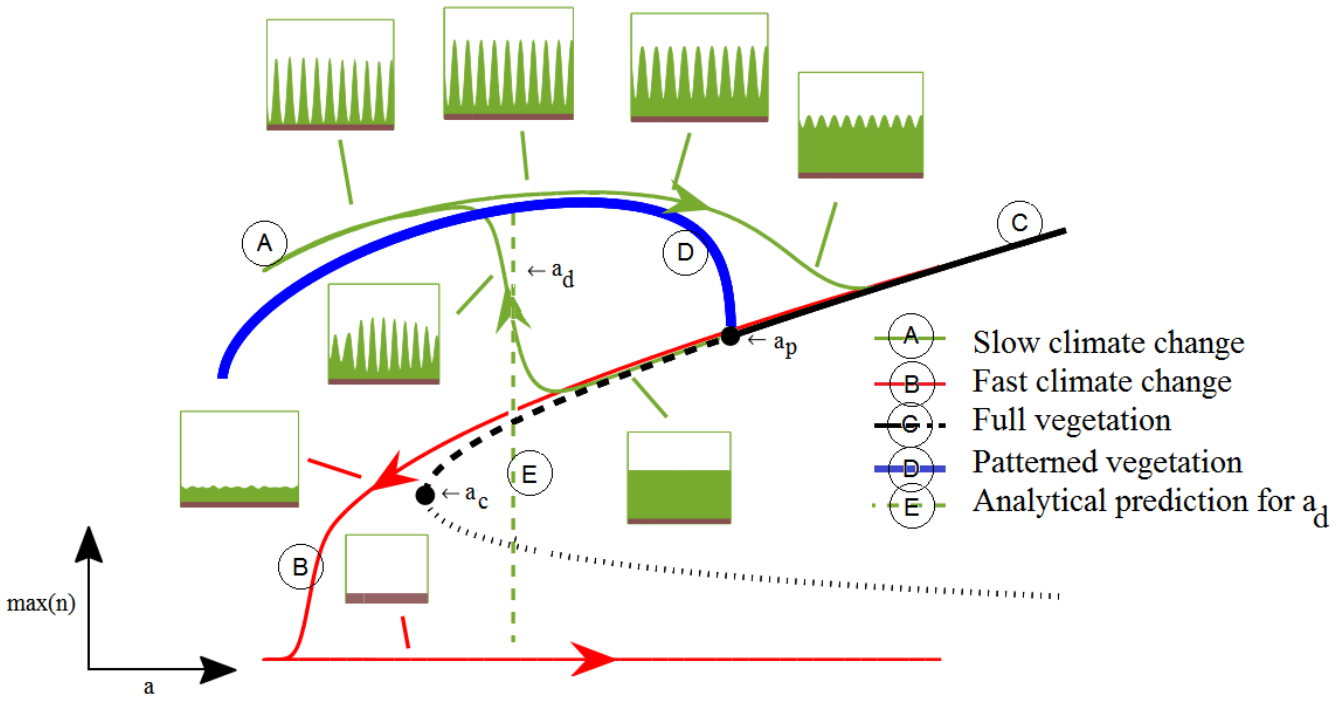


FIG. 1. (colour online) Evolution of vegetation patterns in the presence of slow precipitation drift. The green curve A avoids the tipping point by going into a reversible patterned state. The red curve B falls off the fold point leading to irreversible extinction. Model (1) is used with $a$ given by (5). The Green curve A corresponds to slow decrease ($\varepsilon = 0.006$, corresponding to a change of 2 mm/year) while the red curve B corresponds to a faster decrease ($\varepsilon = 0.03$, corresponding to a change of 40 mm/year). Other parameters are $a_0 = 2.85, a_1 = 1.75, \sigma_0 = 0.0001, \delta = 0.05, d = 1, c = 0$ on a domain of size $L = 22.839$ with periodic boundary conditions. The full vegetation state (black curve C) bifurcates into a patterned state (blue curve D, computed by the software package AUTO [22]) at $a = a_p = 2.4743$, and has a fold point at $a_c = 2$. For values of $a$ below $a_p$ and above $a_c$, the full vegetation state still exists (dashed black curve C) but is unstable to spatial perturbations. The vertical green dashed line E at $a = a_d = 2.18$ is the asymptotic prediction for the delayed "take-off" value of the green curve. Excellent agreement between the asymptotics and numerics is observed.

corresponding to the rate at which precipitation is decreased as a result of climate change or gradual drought onset. The noise represents fluctuations in precipitation due to weather or seasonal variability. We model it using

$$\text{noise} = \sigma_0 \frac{dW}{dt}, \tag{3}$$

where $dW_t$ is spatio-temporal Weiner process, defined by (see e.g. [32–34])

$$dW = \sqrt{dt} \sum_{m=-\infty}^{\infty} \xi_m(t) \exp(imx); \tag{4}$$

here $\xi_m(t)$ is a Gaussian random variable (with mean zero and variance one). Furthermore we assume that $dW$ is real, so that $\xi_{-m} = \overline{\xi_m}$. See Appendix A for numerical implementation details. The noise drives a spatial instability and plays an essential role in transitioning the system to a heterogeneous state, thus allowing the formation of localized vegetation patches and increasing resilience to drought.

Alternatively, to model precipitation that varies periodically between $a_0$ and $a_1$ we take

$$a = a_0 + (a_1 - a_0)(1 - \cos(\varepsilon t))/2 + \text{noise}. \tag{5}$$

We illustrate our main point in Figure 1. We let precipitation vary periodically according to (5), with green (A) and red (B) curves corresponding to two distinct values of $\varepsilon$ as given in the caption (colour online). The nontrivial spatially homogeneous steady state corresponding to full vegetation cover is shown by the black curve (C). It exhibits a tipping-point structure at $a = a_c$. Below the critical precipitation rate $a = a_c$, the only spatially homogeneous state is $n = 0$, corresponding to a "desert state". On the other hand, the patterned state – shown in blue (D) – bifurcates

off the full vegetation state at $a = a_p$ (as a result of a Turing bifurcation), and exists even for precipitation rates well below $a_c$.

As $a$ slowly drifts below $a_p$, the homogeneous state becomes unstable to spatial perturbations. However, it takes time for these perturbations to grow, as illustrated in Figure 1. If the drift speed $\varepsilon$ is too large (for example, as a result of rapid onset of drought), represented by the red curve (B), or equivalently, if the spatial noise $\sigma_0$ is sufficiently small, the perturbations may not have enough time to grow before the tipping point $a_c$ is reached. If this happens, the tipping point will be activated *before* the system can transition to the patterned state. In this case the plant population crashes to zero, resulting in rapid desertification (extinction). Moreover, as is usual with tipping points, this process is not easily reversible, so the desert state persists even as precipitation later increases back to the regime that supports full vegetation cover $(a > a_p)$.

By contrast, if the drift speed $\varepsilon$ is sufficiently small (for example, due to a naturally occurring climate change), represented by the green curve (A), or equivalently, if the spatial noise $\sigma_0$ is sufficiently large, there is enough time for the spatial perturbations to grow, and the system is able to transition to the patterned state. This state extends beyond the tipping point $a_c$, which means that the vegetation can persist in a patterned state even as $a$ is decreased below $a_c$. Furthermore, unlike the scenario illustrated by the red curve, the case illustrated by the green curve is entirely reversible: if in the future the precipitation increases past $a_p$, the patterned state gradually transitions back into the full vegetation state.

We have modeled and analyzed this phenomenon using a stochastic ODE that describes the evolution of the system along each of the Fourier modes near the slowly-varying steady state. The resulting equation is a variant of the Ornstein-Uhlenbeck process. For each mode, the combined effect of the slow drift and noise determines the solution spread of the associated Fokker-Planck equation, which describes the probability density associated to the solutions of the underlying stochastic ODE. Using a computation similar to that in [35, 36], we derived an analytical threshold at which the variance of this density starts to grow exponentially. The end result is the prediction, $a_d$, for the delayed "take-off" value at which the system transitions to the patterned Turing state. See the next section for details and precise definition of $a_d$. This threshold is indicated by vertical dashed lines at respective values of $a = a_d$ in Figures 1 and 2. For sufficiently large $\varepsilon$, $a_d$ does not exist, indicating that the transition cannot occur, resulting in extinction. Figure 1 illustrates an excellent agreement between this analytic prediction and the full numerical simulation of the system.

It has been known for a long time that a slow parameter drift induces a delay in bifurcation [37, 38]. Recent studies have shown that noise also plays a key role in the resilience of a homogeneous state against tipping points, and several effects have been described, including bifurcation-driven tipping [15, 16, 39–41], noise-induced tipping [42–45], and rate-dependent tipping [46]. Delayed bifurcations with noise have been studied in the context of stochastic ODE's [35, 36, 47] with applications to climate change [45, 48, 49], laser dynamics [50] and neuronal bursting [51], among others; see also [52] for an overview. All of these works study systems described by stochastic ODE's with a parameter drift. By contrast, very little work has been done on slow passage problems in PDE's with noise. However, see recent work [53] where some related questions are studied. In particular, we show that the spatial component of the PDE system, when combined with noise and parameter drift, plays a key role in preventing activation of the tipping point.

## MATHEMATICAL ANALYSIS OF THE EFFECT OF NOISE

Our starting point is the system (1), where we take $a = a(\varepsilon t) + \text{noise}$ and noise is spatio-temporal Gaussian white noise with zero mean and standard deviation of $\sigma_0$. For pedagogical reasons, we will assume that both $b$ and $c$ are small and can be discarded and we scale $d$ to 1 (the analysis below can be modified to incorporate a more general case that exhibits the same phenomenon; we expect to report on the more general case elsewhere soon). The system (1) then becomes

$$\frac{dn}{dt} = \delta \frac{d^2 n}{dx^2} - n + wn^2 \,, \tag{6a}$$

$$0 = \frac{d^2 w}{dx^2} + a(\varepsilon t) - w - wn^2 + \sigma_0 \frac{dW}{dt} \,, \tag{6b}$$

where the spatio-temporal noise $dW$ is defined in (4). For a constant $a$ and with $\sigma_0 = 0$, the steady-state solution structure is shown in Figure 2 in black; it has a fold point at $a = a_c = 2$. For $a > a_c$, there are three solutions: $n = 0, w = a$ and

$$n_\pm = a/2 \pm \sqrt{a^2/4 - 1} \,, \qquad w_\pm = 1/n_\pm \,. \tag{7}$$

For $a < a_c$, the only *spatially homogeneous* solution is the desert state $n = 0$. Standard linear analysis shows that the steady state $n_-$ is unstable, whereas $n_+$ is stable with respect to spatially uniform perturbations. However $n_+$ undergoes a Turing instability to a patterned state at $a = a_p$ given by

$$a_p = \frac{3 - 2\sqrt{2 - 2\delta}}{\sqrt{\left(3 - 2\sqrt{2 - 2\delta} - \delta\right)\delta}}\,. \tag{8}$$

The dominant Turing branch is shown in blue in Figure 1. In the case where $a$ is slowly-varying with time, $n_\pm$ is a quasi-equilibrium state, $n_+ = n_+(\varepsilon t)$, given by (7) with $a$ replaced by $a(\varepsilon t)$. Linearizing near the quasi-equilibrium, we write

$$n(x,t) = n_+(\varepsilon t) + \phi(x,t)\,, \qquad w(x,t) = w_+(\varepsilon t) + \psi(x,t)\,,$$

with $|\phi|, |\psi| \ll 1$, yielding

$$\frac{d\phi}{dt} + \varepsilon n_+'(\varepsilon t) = \delta\frac{d^2\phi}{dx^2} + \phi + n_+^2\psi\,, \tag{9a}$$

$$0 = \left[\frac{d^2\psi}{dx^2} + \left(-1 - n_+^2\right)\psi - 2\phi\right]dt + \sigma_0 dW\,. \tag{9b}$$

We now separate variables in space. We write

$$\phi(x,t) = \sum \phi_m(t)\, e^{imx}\,, \quad \psi(x,t) = \sum \psi_m(t)\, e^{imx}\,,$$

where the sums are taken over all $m$ such that $m2\pi/L$ is an integer, where $L$ is the length of the domain, which we take to be periodic. Similarly, we decompose the noise in terms of the same Fourier modes and each Fourier coefficient is again Gaussian distributed with zero mean and standard deviation $\sigma_0\sqrt{dt}$. The term $n_+'(\varepsilon t)$ in (9a) is constant in space and therefore does not contribute to any non-zero ($m \neq 0$) modes. We obtain for $m \neq 0$, after dropping the subscripts,

$$\frac{d\phi}{dt} = -m^2\delta\phi + \phi + n_+^2\psi, \tag{10a}$$

$$0 = \left[-m^2\psi + \left(-1 - n_+^2\right)\psi - 2\phi\right]dt + \sigma_0\sqrt{dt}\xi. \tag{10b}$$

Solving for $\psi$ in (10b) and substituting back into (10a), we obtain

$$d\phi = \alpha\left(\varepsilon t\right)\phi dt + \beta\left(\varepsilon t\right)\sqrt{dt}\xi\,, \tag{11a}$$

where $\xi$ is a Gaussian random variable with mean zero and variance 1 and where

$$\alpha\left(s\right) = -m^2\delta + 1 - \frac{2n_+^2\left(s\right)}{m^2 + 1 + n_+^2\left(s\right)}\,, \tag{11b}$$

$$\beta\left(s\right) = \frac{\sigma_0 n_+^2\left(s\right)}{m^2 + 1 + n_+^2\left(s\right)}\,. \tag{11c}$$

Equation (11a) is a variant of an Ornstein–Uhlenbeck process, with coefficients that are slowly changing in time.

In the absence of noise/parameter drift, the mode $m$ is unstable whenever $\alpha > 0$. The Turing bifurcation threshold (8) is obtained by setting $\alpha = 0 = \partial\alpha/\partial m$ and eliminating $m$ from the resulting system. However, the combined effect of slow drift and noise introduce a "delay" in the bifurcation. To compute this delay, we proceed similarly to [35, 36] by studying the density distribution $u\left(\phi, s\right)$ associated with (11a). More precisely, the integral $\int_{\phi_1}^{\phi_2} u(\phi, s)d\phi$ is by definition the probability that $\phi(s) \in (\phi_1, \phi_2)$. The density satisfies the Fokker-Planck PDE given by

$$\varepsilon\frac{\partial}{\partial s}u + \alpha(s)\frac{\partial}{\partial\phi}\left(\phi u\right) = \frac{\beta^2(s)}{2}\frac{\partial^2 u}{\partial\phi^2}\,, \tag{12}$$

with initial condition $\phi(0) = 0$ in (11a) corresponding to $u(\phi, 0) = \delta(\phi)$, where $\delta(z)$ is the Dirac delta function. In (12), we have let $s$ denote the slow time $\varepsilon t$.

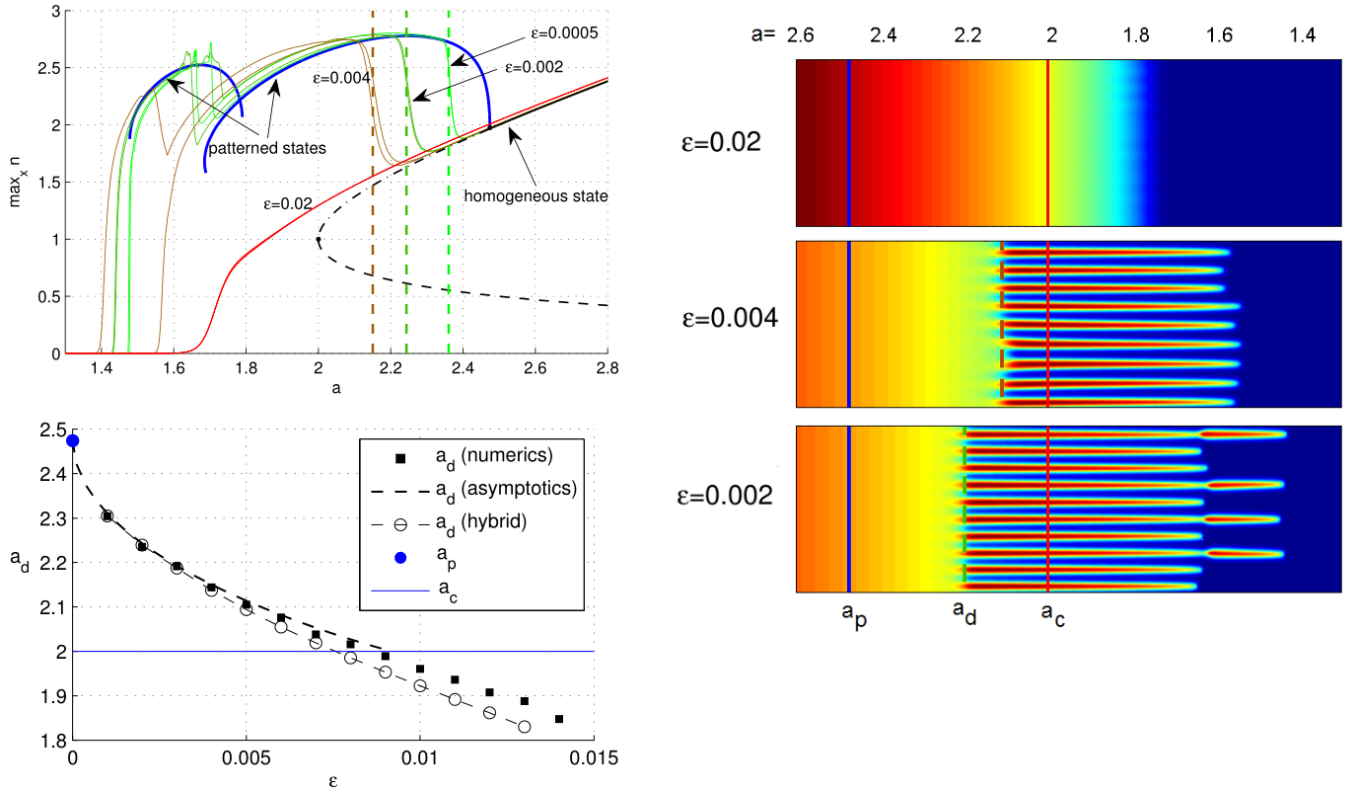


FIG. 2. Numerical verification of $a_d$ as given in (16) for (6). The slow drift is taken to be $a = a_0 - \varepsilon t$ with $a_0 = 3$, $\sigma_0 = 0.0001, L = 22.839$ and $\delta = 0.05$. Top left: the evolution of max $n$ as a function of $a$ with $\varepsilon$ as indicated. The dashed lines show $a_d$ as given by (16). The patterned state (blue on-line) to the left corresponds to a single-bump solution, whereas the patterned state on the right corresponds to the wave-number 10 born from a Turing bifurcation at $a = a_p = 2.47439$. Top right: color plot of $n(x,t)$ as it evolves in time. The Turing bifurcation point $a_p$, the delayed bifurcation $a_d$ and the fold point $a_c = 2$ are indicated. Bottom left: Comparison of asymptotic and full numerical results for $a_d$. The hybrid curve is obtained by using the full homogeneous state (17) instead of (7) when computing (16). The value of $a_d$ is estimated numerically as discussed in the text, and an average over 50 simulations is used. We used $N = 100, dt = 0.1$ (see Appendix A for numerical implementation details).

Equation (12) can be transformed into a standard diffusion equation $v_S = v_{\xi\xi}$ subject to initial condition $v(\xi,0) = \delta(\xi)$ via a change of variables $\xi = \phi \exp\left(-\frac{1}{\varepsilon}\int_0^s \alpha(\rho)d\rho\right)$, $S = \int_0^s \frac{\beta^2(\hat{s})}{2\varepsilon} \exp\left(-\frac{2}{\varepsilon}\int_0^{\hat{s}} \alpha(\rho)d\rho\right) d\hat{s}$, and $u(\phi,t) = \exp\left(-\frac{1}{\varepsilon}\int_0^s \alpha(\rho)d\rho\right) v(\xi,S)$. The solution for $v(\xi,S)$ is simply the fundamental solution of the diffusion equation $v(\xi,S) = \frac{1}{\sqrt{4\pi S}} e^{-\xi^2/(4S)}$. This allows us to explicitly compute the variance in $\phi$, $\sigma^2(s) = \int_{-\infty}^{\infty} \phi^2 u(\phi,s)\, d\phi$, to obtain

$$\sigma^2(s\,;m) = \int_0^s \beta^2(\tau) \exp\left(-\frac{2}{\varepsilon}\int_\tau^s \alpha(\rho)d\rho\right) d\tau. \tag{13}$$

Let $s_p$ be the such that that $\alpha(s_p) = 0$, and we assume that $\alpha'(s_p) > 0$. That is, $s_p$ is the point at which the mode $m$ becomes unstable. Then for $s > s_p$, Laplace's method [54] yields

$$\sigma(s;m) \sim \exp\left(\frac{1}{\varepsilon}\int_{s_p}^s \alpha(\tau)d\tau\right) \beta(s_p) \left(\frac{\pi}{\varepsilon\alpha'(s_p)}\right)^{1/4}, \tag{14}$$

where the dependence of $\sigma$ on $m$ is through that of $\alpha$ and $\beta$ in (11b) and (11c). We define the "take-off" time $s_d = s_d(m)$ for the mode $m$ to be such that $\sigma(s_d;m) = 1$. Alternatively, $s_d$ is such that $\sigma \ll 1$ when $s < s_d$ and $\sigma \gg 1$ when $s > s_d$. For a fixed mode $m$, the value of $s_d$ is therefore found by solving simultaneously

$$\alpha(s_p) = 0; \tag{15a}$$

$$\int_{s_p}^{s_d} \alpha(s)ds + \varepsilon \log\left(\beta(s_p)\left(\frac{\pi}{\varepsilon\alpha'(s_p)}\right)^{1/4}\right) = 0\,. \tag{15b}$$

Equation (15) yields the time $s_d$ at which the solution density spread $\sigma$ for a given mode $m$ starts to grow exponentially fast. Similar results – in the context of stochastic ODE's and for different applications – were derived using a related approach in [35], and also in [36] without using the density formulation (12). Analogous results for linear $\alpha(s)$ and constant $\beta$ were also obtained in [50, 55, 56] using a similar analysis.

Note that, depending on the parameters, a solution for $s_d$ in (15) may not exist, in which case the corresponding mode $m$ is never activated. The first mode that gets activated yields the delayed take-off value for $a$:

$$a_d \equiv a(\min_m s_d(m)), \tag{16}$$

where the minimum is taken over all admissible modes $m$. These are the modes for which the solution to the system (15) exists. If no such modes exist, no take-off value of $a$ exists, and the patterned state is never activated.

Figure 2 compares the analytic prediction (16) for $a_d$ and the delayed value $a_{d,num}$ as estimated from direct numerical simulations of (6). To determine the latter, we first define $t_{d,num}$ as the time at which $(\max_x n - \min_x n)/\operatorname{mean}_x(n)$ first exceeds 1. We then calculate $a_{d,num} = a(\varepsilon t_{d,num})$. We note that, while the threshold of 1 is somewhat arbitrary, halving it has a negligible effect on $a_{d,num}$. Figure 2 also shows two simulations for four different values of $\varepsilon$ each with different random seeds. The bunching together of take-off points for each $\varepsilon$ illustrates that $a_d$ is insensitive to the particular seed chosen. Good agreement is observed between asymptotics and numerics when $a_d$ is above the critical point $a_c = 2$.

Asymptotics as shown in Figure 2 (bottom left) predict extinction for $\varepsilon > 0.09$. However, for the values of $\varepsilon \in (0.009, 0.014)$, full numerical simulations show that homongeneous quasi-state jumps to the patterned state branch even when $a$ has been decreased to below $a_c = 2$ where the homogeneous steady state no longer exists. This is due to the presence of slow relaxation dynamics: it is well known (see for example [57], chapter 6.5) that there is a boundary layer of $O(\varepsilon^{1/3})$ near the fold point, so that the homogeneous state "falls off" not exactly at the fold point, but within $O(\varepsilon^{1/3})$ of it. This delay is readily apparent in Figure 2, where the numerics and asymptotics diverge near $a = 2$. To better capture this behaviour (and thus to better approximate the values of $\varepsilon$ for which the extinction is observed), it suffices to replace the quasi-steady state approximation $n_+$ and $w_+$ in (7) by the solution to the (slowly-evolving) homogeneous (ODE) system

$$\frac{dn}{dt} = -n + wn^2\,, \quad 0 = a(\varepsilon t) - w - wn^2. \tag{17}$$

Moreover, it is no longer true that $n_+w_+ = 1$ so that equations (11b, 11c) and $\alpha, \beta$ are replaced by

$$\alpha\,(s) = -m^2\delta + (2wn - 1) - \frac{2wn}{m^2 + 1 + n^2}\,, \tag{18a}$$

$$\beta\,(s) = \frac{\sigma_0 n^2}{m^2 + 1 + n^2}\,. \tag{18b}$$

With this modification, the computation for $a_d$ is carried out as in before. This allowed us to better capture the transition (or non-transition) to the patterned state even slightly below the tipping point $a = a_c$. This is clearly shown in the curve labeled "hybrid" and its agreement with the full numerical result in Figure 2 (bottom left).

To simplify the exposition, we have assumed that $b = c = 0$ in (6). However our method can be generalized to remove these assumptions. If $c \neq 0$ then $\alpha$ in (11b) is complex; in this case the analysis proceeds as before but with $\alpha$ replaced by its real part. The case $b \neq 0$ is more involved. In this case, $\alpha$ is an eigenvalue of a certain 2x2 matrix; and furthermore the formula for $\beta$ depends on an adjoint eigenvector of such a matrix. Moreover there is a Hopf bifurcation possible when $b$ is too large. This is a work in progress and we expect to report the results of this soon.

Our method should also be applicable to more complex models of patterned vegetation, such those described in [27, 58–62]; and more broadly to a general class of reaction-diffusion PDEs that have a Turing bifurcation leading to pattern formation.

As shown in Figure 2, the Turing branch can also undergo a secondary bifurcation: it eventually becomes unstable, leading to a "coarsening" process that results in fewer number of localized regions [31, 63]. Whether the secondary bifurcation is activated depends on the speed of the drift as Figure 2 illustrates: when $\varepsilon = 0.002$, the solution has time to coarsen and persists beyond the fold point of the Turing branch. By contrast, when $\varepsilon = 0.004$, the fold point

of the Turing branch is reached before the coarsening process is realized. For localized states, a similar phenomenon in the absence of noise was recently studied in [64]. It would be interesting to extend these results to incorporate the role of noise on these secondary bifurcations.

In conclusion, we have used a simple mathematical model to illustrate how patterned states can provide a refuge and prevent extinction under stressed conditions, even as the control parameter falls below the tipping point of a homogeneous state. The patterned state can recover to the full vegetation state when the control parameter is dialed back to favorable conditions. However, if the control parameter drifts too quickly toward threatening conditions, the system may have no time to transition to the patterned state before the tipping point is reached, resulting in an irreversible extinction. This simple mechanism underscores the key role that spatial heterogeneity and noise have on the resilience of the system. It also illustrates the importance of not only the absolute level of climate change, but also the *speed* with which it occurs.

## APPENDIX A: NUMERICAL METHOD

We use finite differences to solve (6) numerically. Because simulating PDE's with noise is not as standard, we include here the algorithm and Matlab code to do this, in particular the details of how to implement the spatio-temporal noise correctly.

Discretize in space using $N$ gridpoints, $\Delta x = L/N$, and in time using stepsize $\Delta t$ so that $w(x_k, t_j) \approx w_j^k$, $n(x,t) \approx n_j^k$ where $x_k = \Delta x k$ with $k = 1 \dots N$, $t_j = \Delta t j$. We use a simple implicit-explicit Euler scheme as follows:

$$\frac{n_{j+1}^k - n_j^k}{\Delta t} = \delta \frac{n_{j+1}^{k+1} + n_{j+1}^{k-1} - 2n_{j+1}^k}{(\Delta x)^2} - n_{j+1}^k + w_j^k \left(n_j^k\right)^2,$$

$$0 = \frac{w_{j+1}^{k+1} + w_{j+1}^{k-1} - 2w_{j+1}^k}{(\Delta x)^2} + a(\varepsilon t_j) - w_j^k - w_j^k \left(n_j^k\right)^2 + \sigma_0 \frac{1}{\Delta t} W_j^k.$$

Here, $W_j^k$ is the discretization of the noise term. Care must be taken to truncate the infinite series (4) to $N$ modes to avoid oversampling:

$$W_j^k = \sqrt{\Delta t} \sum_{m=-N/2+1}^{N/2} \xi_m(t_j) e^{imx_k}, \tag{19}$$

where $\xi_{-m} = \overline{\xi_m}$ when $m < 0$, and $\xi_m(t_k) = X + iY$ with $X, Y$ normal random variable of mean zero and variance 1 when $m > 0$; and $N$ is assumed to be even. This can be implemented via discrete FFT.

Alternatively, note from the definition (19) that $W_j^k$ is normally distributed (since it is a sum of normal variables), that its mean is zero and its variance is given by

$$var(W_j^k) = \Delta t N.$$

Hence an equivalent definition of $W_j^k$, and the one we will use, is

$$W_j^k = \sqrt{\Delta t}\sqrt{N}\xi_j(t_k) \tag{20}$$

where $\xi_j(t_k)$ is a real Gaussian random variable. We include self-contained matlab code – see figure 3 – with further implementation details.

*Acknowledgments*

We are grateful to the anonymous referees for suggestions which improved the paper significantly. We thank Mary Silber for useful discussions and suggestions. Y. Chen was supported in part by the NSF Math and Climate Research Network (DMS-0940262). T. Kolokolnikov was supported by NSERC Discovery Grant No. RGPIN-33798 and Accelerator Supplement Grant No. RGPAS/461907. J. C. Tzou was supported by an AARMS Postdoctoral Fellowship.

[1] P. N. Pearson and M. R. Palmer, Nature **406**, 695 (2000).

```
N=200;
L=22.839;
x=linspace(0,L,N);

delta=0.05;
sigma0=0.0001;
eps=0.005;
a0=3;
a1=1.3;
dt=0.1;
T=(a0-a1)/eps;
tt=0:dt:T;
aa= a0-eps*tt;

n0=a0/2+sqrt(a0^2/4-1);
n=(x') *0+n0; w=1./n;

dx=x(2)-x(1);

tout=0;

Lap=-2*diag(ones(1,N))+diag(ones(1,N-1),1)+diag(ones(1,N-1),-1);
Lap(1,2)=2;Lap(N,N-1)=2;

M1=delta*Lap/dx^2+eye(N)*(-1/dt-1);
M2=Lap/dx^2-eye(N);

maxn=[];spread=[];
for idx=1:numel(tt)
    a=aa(idx);
    t=tt(idx);

    noise=randn(N,1)*sqrt(dt)*sigma0*sqrt(N);
    wnext=(M2-diag(n.^2))\(-a-noise/dt);
    nnext=M1\(-n/dt-n.^2.*w);
    n=nnext; w=wnext;

    maxn(end+1)=max(n);
    spread(end+1) = (max(n)-min(n))/mean(n);

    if t>tout
        tout=tout+10;
        subplot(2,1,1);
        plot(x,n,x,w);
        legend('n','w'); xlabel('x');
        title(sprintf('t=%g a=%g',t, a));
        drawnow;
    end;
end;

%%

subplot(2,1,2);  hold on;
plot(aa,maxn);
at = interp1( spread, aa, 1);
plot([at,at],[0,3],'--b');
xlabel('a'); ylabel('max(n)');
title(sprintf('a_d=%g',at));
```

FIG. 3. Code for simulating (6) with $a = a_0 - \varepsilon t + \sigma_0 \frac{dW}{dt}$. Copy and paste into matlab to run.

[2] S. Solomon *et al.*, Intergovernmental Panel on Climate Change, Group I (2007).
[3] J.-R. Petit, J. Jouzel, D. Raynaud, N. I. Barkov, J.-M. Barnola, I. Basile, M. Bender, J. Chappellaz, M. Davis, G. Delaygue, *et al.*, Nature **399**, 429 (1999).
[4] C. Turley, J. Blackford, S. Widdicombe, D. Lowe, P. Nightingale, and A. Rees, Avoiding dangerous climate change **8**, 65 (2006).
[5] H. Schellnhuber *et al.*, *Turn down the heat: climate extremes, regional impacts, and the case for resilience.*, International Bank for Reconstruction and Development, World Bank (2013).
[6] M. Hofmann and H.-J. Schellnhuber, Proceedings of the National Academy of Sciences **106**, 3017 (2009).
[7] W. Foden, G. F. Midgley, G. Hughes, W. J. Bond, W. Thuiller, M. T. Hoffman, P. Kaleme, L. G. Underhill, A. Rebelo, and L. Hannah, Diversity and Distributions **13**, 645 (2007).
[8] T. P. Hughes, A. H. Baird, D. R. Bellwood, M. Card, S. R. Connolly, C. Folke, R. Grosberg, O. Hoegh-Guldberg, J. Jackson, J. Kleypas, *et al.*, science **301**, 929 (2003).
[9] O. Hoegh-Guldberg, P. Mumby, A. Hooten, R. Steneck, P. Greenfield, E. Gomez, C. Harvell, P. Sale, A. Edwards, K. Caldeira, *et al.*, science **318**, 1737 (2007).
[10] J. Travis, Proceedings of the Royal Society of London. Series B: Biological Sciences **270**, 467 (2003).
[11] K. Siteur, E. Siero, M. B. Eppinga, J. D. Rademacher, A. Doelman, and M. Rietkerk, Ecological Complexity **20**, 81 (2014).
[12] C. B. Field, V. Barros, T. F. Stocker, and Q. Dahe, *Managing the Risks of Extreme Events and Disasters to Advance Climate Change Adaptation: Special Report of the Intergovernmental Panel on Climate Change* (Cambridge University Press, 2012).
[13] A. Dai, K. E. Trenberth, and T. Qian, Journal of Hydrometeorology **5**, 1117 (2004).
[14] K. E. Trenberth, Climate Research **47**, 123 (2011).
[15] J. T. Overpeck and J. E. Cole, Annu. Rev. Environ. Resour. **31**, 1 (2006).
[16] T. M. Lenton, H. Held, E. Kriegler, J. W. Hall, W. Lucht, S. Rahmstorf, and H. J. Schellnhuber, Proceedings of the National Academy of Sciences **105**, 1786 (2008).
[17] S. R. Carpenter, J. J. Cole, M. L. Pace, R. Batt, W. Brock, T. Cline, J. Coloso, J. R. Hodgson, J. F. Kitchell, D. A. Seekell, *et al.*, Science **332**, 1079 (2011).
[18] M. Scheffer, J. Bascompte, W. A. Brock, V. Brovkin, S. R. Carpenter, V. Dakos, H. Held, E. H. van Nes, M. Rietkerk, and G. Sugihara, Nature **461**, 53 (2009).
[19] V. Guttal and C. Jayaprakash, Ecology Letters **11**, 450 (2008).
[20] J. E. Tierney *et al.*, Science **342**, 843 (2013).
[21] S. K. Praetorius and A. C. Mix, Science **345**, 444 (2014).
[22] E. J. Doedel, A. R. Champneys, T. F. Fairgrieve, Y. A. Kuznetsov, B. Sandstede, and X. Wang, "Auto 97: Continuation and bifurcation software for ordinary differential equations (with homcont),".
[23] C. Shisanya, C. Recha, A. Anyamba, *et al.*, International Journal of Geosciences **2**, 36 (2011).
[24] J. A. Sherratt, Ecological Complexity **14**, 8 (2013).
[25] C. A. Klausmeier, Science **284**, 1826 (1999).
[26] S. Kéfi, M. Rietkerk, C. L. Alados, Y. Pueyo, V. P. Papanastasis, A. ElAich, and P. C. De Ruiter, Nature **449**, 213 (2007).
[27] J. Von Hardenberg, E. Meron, M. Shachak, and Y. Zarmi, Physical Review Letters **87**, 198101 (2001).
[28] M. Boer and J. Puigdefábregas, Earth Surface Processes and Landforms **30**, 149 (2005).
[29] M. Rietkerk, S. C. Dekker, P. C. de Ruiter, and J. van de Koppel, Science **305**, 1926 (2004).
[30] J. A. Sherratt and G. J. Lord, Theoretical population biology **71**, 1 (2007).
[31] S. van der Stelt, A. Doelman, G. Hek, and J. D. Rademacher, Journal of nonlinear science **23**, 39 (2013).
[32] T. Shardlow, Electronic Journal of Differential Equations **2000**, 1 (2000).
[33] M. Hairer, M. D. Ryser, and H. Weber, Electron. J. Probab **17**, 1 (2012).
[34] M. D. Ryser, N. Nigam, and P. F. Tupper, Journal of Computational Physics **231**, 2537 (2012).
[35] R. Kuske, Journal of statistical physics **96**, 797 (1999).
[36] N. Berglund and B. Gentz, Probability theory and related fields **122**, 341 (2002).
[37] P. Mandel and T. Erneux, Journal of statistical physics **48**, 1059 (1987).
[38] S. M. Baer, T. Erneux, and J. Rinzel, SIAM Journal on Applied mathematics **49**, 55 (1989).
[39] R. M. May, Nature **269**, 471 (1977).
[40] V. Dakos, M. Scheffer, E. H. van Nes, V. Brovkin, V. Petoukhov, and H. Held, Proceedings of the National Academy of Sciences **105**, 14308 (2008).
[41] M. Scheffer, S. Carpenter, J. A. Foley, C. Folke, and B. Walker, Nature **413**, 591 (2001).
[42] C. Kuehn, Physica D: Nonlinear Phenomena **240**, 1020 (2011).
[43] A. Sutera, Quarterly Journal of the Royal Meteorological Society **107**, 137 (1981).
[44] K. Hasselmann, Progress in Oceanography **11**, 69 (1982).
[45] J. M. T. Thompson and J. Sieber, IMA Journal of Applied Mathematics **76**, 27 (2011).
[46] P. Ashwin, S. Wieczorek, R. Vitolo, and P. Cox, Philosophical Transactions of the Royal Society A: Mathematical, Physical and Engineering Sciences **370**, 1166 (2012).
[47] K. M. Jansons and G. Lythe, Journal of statistical physics **90**, 227 (1998).
[48] P. D'Odorico, F. Laio, and L. Ridolfi, Proceedings of the National Academy of Sciences of the United States of America **102**, 10819 (2005).
[49] P. D'Odorico and A. Bhattachan, Philosophical Transactions of the Royal Society B: Biological Sciences **367**, 3145 (2012).

[50] M. Torrent and M. San Miguel, Physical Review A **38**, 245 (1988).
[51] R. Kuske and S. Baer, Bulletin of mathematical biology **64**, 447 (2002).
[52] B. Lindner, J. Garcıa-Ojalvo, A. Neiman, and L. Schimansky-Geier, Physics Reports **392**, 321 (2004).
[53] K. Gowda and C. Kuehn, arXiv preprint arXiv:1403.5920 (2014).
[54] C. M. Bender and S. A. Orszag, *Advanced mathematical methods for scientists and engineers I: Asymptotic methods and perturbation theory*, Vol. 1 (Springer, 1999).
[55] N. Stocks, R. Mannella, and P. V. McClintock, Physical Review A **40**, 5361 (1989).
[56] H. Zeghlache, P. Mandel, and C. Van den Broeck, Physical Review A **40**, 286 (1989).
[57] M. H. Holmes, *Introduction to perturbation methods*, Vol. 20 (Springer Science & Business Media, 2012).
[58] E. Meron, E. Gilad, J. von Hardenberg, M. Shachak, and Y. Zarmi, Chaos, Solitons & Fractals **19**, 367 (2004).
[59] E. Meron, H. Yizhaq, and E. Gilad, Chaos: An Interdisciplinary Journal of Nonlinear Science **17**, 037109 (2007).
[60] A. Kletter, J. Von Hardenberg, E. Meron, and A. Provenzale, Journal of theoretical biology **256**, 574 (2009).
[61] O. Lejeune, M. Tlidi, and P. Couteron, Physical Review E **66**, 010901 (2002).
[62] V. Breña-Medina, D. Avitabile, A. Champneys, and M. Ward, arXiv preprint arXiv:1403.5318 (2014).
[63] T. Kolokolnikov, M. J. Ward, and J. Wei, Studies in Applied Mathematics **115**, 21 (2005).
[64] J. C. Tzou, M. J. Ward, and T. Kolokolnikov, Physica D: Nonlinear Phenomena **290**, 24 (2015).